

**COB-2025-0123**

## **EXPERIMENTAL AND COMPUTATIONAL EVALUATION OF AN AUTOMOTIVE AIR-CONDITIONING SYSTEM**

**Guilherme Medeiros de Córdova**

**Diogo Lôndero da Silva**

ReVe - Vehicular Refrigeration Laboratory, Mobility Engineering Department, Federal University of Santa Catarina, Joinville, SC, Brazil.

guilhermemcordova@gmail.com, diogo.londero@ufsc.br

**Abstract.** *This study aims to evaluate the thermal performance of an automotive air-conditioning system based on experimental results and a computational model. Experimental data were collected using a full-scale passenger car tested in a climatic aerodynamic wind tunnel capable of replicating real-world operating conditions. The computational model is developed based on thermodynamic and heat transfer principles. An iterative procedure is used to determine the operating conditions that satisfy energy conservation, while it accomplishes the refrigerant mass flow provided by the compressor. The accuracy of the computational model was evaluated by comparing its predictions to the experimental results, showing errors below 10% in most results for both power consumption and cooling capacity. The model was employed to assess the thermal performance of refrigerants R-134a and R-1234yf, with the latter showing an average reduction in COP of approximately 2.6%. The model was also employed to assess the impact of a potential condenser geometry modification aimed at mitigating the COP reduction caused by the refrigerant change.*

**Keywords:** *Automotive air-conditioning, Computational model, Experimental results, Climate wind tunnel.*

### **1. INTRODUCTION**

A modern Air-Conditioning (AC) system provides more than cool air, as it is responsible for air filtration, air renovation, humidity control and thermal management of battery packs in electric vehicles. Safety is another important aspect related to the AC system. In addition to improving windshield visibility, studies show that drivers in overheated cabins may experience fatigue and slower reaction times, increasing the risk of accidents (Lahimer *et al.*, 2023). Regardless of significant variations in thermal loads, an automotive air-conditioning system is engineered to ensure thermal comfort and occupant safety, while also addressing constraints such as cost, size, and weight (Da Silva and Melo, 2016).

Automotive air-conditioning is also associated with a significant increase in energy consumption, either in the form of fuel for internal combustion engine vehicles or battery power in electric vehicles (Cordova, 2024). For example, Zhang *et al.* (2018) reported that in combustion engine vehicles using belt-driven compressors, fuel consumption can increase by up to 10%. For electric vehicles, the air-conditioning system can reduce the driving range by 30% up to 40%. Even auxiliary components, such as fans and the electromagnetic clutch, account for more than 10% of the total AC system power consumption depending on the operating condition (Da Silva *et al.*, 2024). This highlights the need to develop highly efficient AC systems to improve energy use, extend vehicle range and minimize pollutant emission levels.

Due to sustainability issues and regulation compliance, low global warming potential refrigerants must be used in new designs. In 2014, the European Union introduced Regulation No. 517/2014 (F-gas Regulation), which mandates a two-third reduction in the use of refrigerants with a Global Warming Potential (GWP) above 150 by 2030. This was followed by the Kigali Amendment to the Montreal Protocol in 2016, which aims to gradually phase down the consumption of high-GWP hydrofluorocarbons (HFCs). For Brazil, the schedule includes freezing HFC consumption in 2024, followed by reductions of 10% by 2029, 30% by 2035, 50% by 2040, and 80% by 2045 (Kigali, 2024).

Among the few viable replacements for R-134a, R-1234yf has emerged as a promising alternative due to its similar thermodynamic properties (Vashisht and Rakshit, 2021). However, given time and cost constraints related to AC system modifications, the automotive industry has increasingly relied on computational modeling to predict system performance (Mendes *et al.*, 2024, Da Silva and Cordova, 2017). Moreover, R-1234yf is also classified as slightly flammable, which requires additional considerations regarding the safety of the vehicle's occupants. Thus, the development and optimization of automotive air-conditioning systems remain challenging due to diverse application environments, globalization of design processes, high cost of experimentation and evolving regulatory frameworks.

Simulation has therefore become a critical tool in the development of automotive air-conditioning systems, enabling engineers to optimize performance, energy efficiency, and thermal comfort while reducing development time and cost (Zhan and Yu, 2022). Advances in multi-physics modeling allow for accurate predictions of airflow, refrigerant behavior, and heat exchange within complex vehicle architectures (Wang *et al.*, 2019; Liu *et al.*, 2025). These tools are essential for evaluating new component designs, refrigerant alternatives, and system behavior under various operational conditions, particularly to comply with increasingly stringent environmental regulations. Therefore, the aim of this study is to evaluate

the thermal performance of an automotive air-conditioning system based on a computational model and experimental results obtained with a full-scale passenger car tested in a climatic aerodynamic wind tunnel.

## 2. EXPERIMENTAL ACTIVITY IN A CLIMATIC AERODYNAMIC WIND TUNNEL

The experimental database was obtained using a compact passenger vehicle equipped with an AC system. This vehicle was tested in a climatic aerodynamic wind tunnel capable of reproducing real operating conditions. The AC system was charged with refrigerant R-134a. Figure 1a presents a schematic of the climatic wind tunnel, which features an underground floor where a roller dynamometer (a) is located. This dynamometer is in contact with the front wheels of the vehicle positioned inside the wind tunnel. The dynamometer speed can be controlled from 0 to 180 km/h and is correlated with the air velocity provided by a fan (b). The air velocity is measured using a Pitot tube positioned at point (c), inside the duct (d) that directs airflow toward the vehicle. On the upper level of the wind tunnel, heat exchangers (e) and air humidifiers (f) are installed, allowing control of the tunnel temperature from  $-20^{\circ}\text{C}$  to  $50^{\circ}\text{C}$  and relative humidity from 30% to 80%. Figure 1b shows the temperature measurement points on the vehicle. The external tube surface temperature's locations are indicated by the letters in Figure 1b, as follows: compressor discharge (a), compressor suction (b), liquid line (c), thermostatic valve inlet (d), and thermostatic valve outlet (e). Air temperatures at the inlet and outlet of the heat exchangers are identified as: condenser inlet (f), evaporator inlet (g), and evaporator outlet (h).

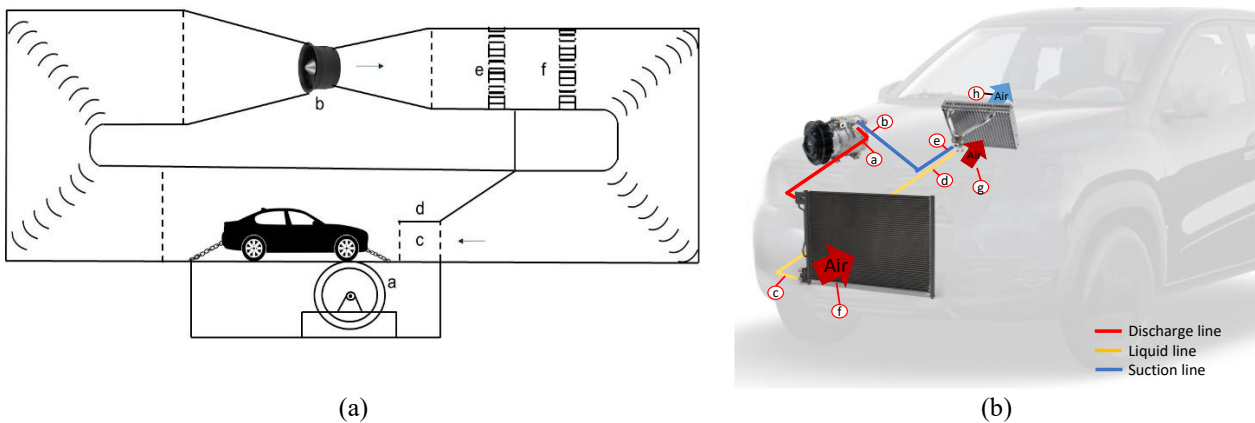


Figure 1. Climatic aerodynamic wind tunnel (a) and AC system temperature measurement points (b).

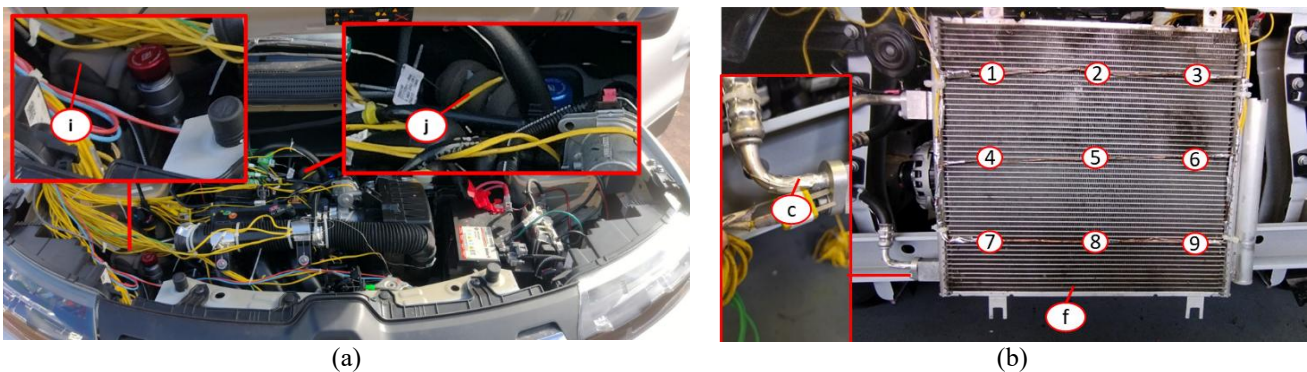


Figure 2. Details of pressure (a) and temperature measurements positions (b), from Cordova (2024).

Moreover, Figure 2a shows the positions where the high-side pressure (i) and low-side pressure (j) were measured using the refrigerant service port valves of the AC system, while Fig. 2b illustrates the position of the thermocouples used to measure the air temperatures (1-9) and the refrigerant temperature (c) at the condenser. The measurement uncertainties of temperature and pressure were  $\pm 0.5^{\circ}\text{C}$  and  $\pm 0.1$  bar, respectively. Using the concept of uncertainty propagation, the uncertainty of the volumetric airflow rate, power consumption and cooling capacity were estimated at  $\pm 10$  m<sup>3</sup>/h,  $\pm 40$  W and  $\pm 200$  W, respectively.

Table 1 presents the experimental plan, related to 14 experimental conditions investigated in this study. For the AC system tests, the climate control unit of the car was set to draw in external air. This configuration enabled steady-state conditions for air admitted into the cabin, without intermittent cycles caused by the disengagement of the compressor's electromagnetic clutch. The velocity of the dynamometer was tested at 40 and 80 km/h. The air temperature was varied between  $45^{\circ}\text{C}$  and  $30^{\circ}\text{C}$ , and relative humidity between 35% and 60%. Another variable in the system was the radial fan speed inside the car HVAC unit, which was adjusted to provide airflow rates between 110 and 280 kg/h.

Table 1. Experimental plan.

Test	Ambient temperature [°C]	Relative humidity [%]	Dynamometer velocity [km/h]	Evaporator air flow rate [kg/h]
1	45.0	35	40	220
2	45.0	35	40	175
3	45.0	35	40	110
4	45.0	35	80	220
5	45.0	35	80	175
6	45.0	35	80	110
7	40.0	40	40	280
8	40.0	40	40	220
9	40.0	40	40	175
10	40.0	40	80	280
11	35.0	50	40	280
12	35.0	50	80	280
13	30.0	60	80	280
14	30.0	60	40	280

### 3. COMPUTATIONAL MODEL

The computational model was developed based on the fundamentals of thermodynamics, fluid mechanics and heat transfer. The proposed model also requires the use of thermodynamic properties of the refrigerant, which defines the thermodynamic states according to the operating condition investigated. The following simplifications were adopted to develop the mathematical model:

- (i) steady-state operation;
- (ii) average heat transfer coefficients in the condenser;
- (iii) semi-empirical model for the compressor;
- (iv) uniform air flow in the condenser;
- (v) pressure drop in the condenser is disregarded.

Additionally, the expansion device and evaporator operating conditions are considered as input data, by imposing the suction pressure and superheat at the compressor suction line. A similar approach was proposed by Hermes *et al.* (2012).

#### 3.1 COMPRESSOR SUBMODEL

A Subros compressor, model 10SL09, swash plate type, was used for the mathematical modeling, which has 10 pistons and a fixed displacement of 90 cm<sup>3</sup>. The mathematical model of the compressor was developed based on Li (2013), using data on refrigeration capacity and power consumption provided by the compressor manufacturer. Thus, the volumetric efficiency ( $\eta_v$ ) of the compressor can be expressed by

$$\eta_v = 1 - \frac{V_m}{V_w} \left[ \left( \frac{p_d}{p_s} \right)^{\frac{1}{n}} - 1 \right], \quad (1)$$

where  $p_d$  is the compressor discharge pressure,  $p_s$  is the suction pressure,  $V_m$  is the dead volume,  $V_w$  is the swept volume of the compressor and  $n$  is the polytropic coefficient.

Li (2013) also presented the dependence relationship between the polytropic coefficient and the ratio between dead volume and swept volume of the compressor, taking the polytropic coefficient as an isentropic coefficient ( $\kappa$ ) and using experimental data. Thus, Equation 1 is reformulated, and the volumetric efficiency ( $\eta_v$ ) of the compressor is expressed by

$$\eta_v = b_1 + b_2 \left[ \left( \frac{p_d}{p_s} \right)^{\frac{1}{\kappa}} \right], \quad (2)$$

where  $b_1$  and  $b_2$  are unknown parameters that are obtained based on experimental data.

Additionally, the compressor refrigerant mass flow rate ( $\dot{m}_{comp}$ ) is calculated by

$$\dot{m}_{comp} = \eta_v \rho_r V_w N, \quad (3)$$

where  $N$  is the compressor rotation per minute and  $\rho_r$  is the refrigerant density at the compressor suction.

Isentropic efficiency ( $\eta_{is}$ ) and the power consumed by the compressor ( $\dot{W}_{comp}$ ) were expressed as

$$\eta_{is} = \frac{(i_{2s} - i_1)}{(i_2 - i_1)}, \quad (4)$$

and

$$\dot{W}_{comp} = \dot{m}_{comp} (i_2 - i_1), \quad (5)$$

where  $i_{2s}$  is the isentropic discharge enthalpy,  $i_2$  is the actual enthalpy at the compressor discharge, and  $i_1$  is the enthalpy in the suction line.

To obtain the discharge enthalpy ( $i_2$ ), the isentropic efficiency ( $\eta_{is}$ ) was regressed as a function of experimental data expressed by

$$\eta_{is} = c_1 + c_2 \left[ \left( \frac{p_d}{p_s} \right)^{\frac{1}{\kappa}} \right], \quad (6)$$

where  $\kappa$  is the polytropic coefficient,  $c_1$  and  $c_2$  are unknown parameters that require experimental data for adjustment.

### 3.2 CONDENSER SUBMODEL

The condenser, depicted in Fig. 3, is made of aluminum alloy, has two passes and external dimensions of 375 x 348 x 12 mm<sup>3</sup>, being  $L_{cond}$  correspondent to the first dimension. Moreover, the condenser has 52 flat tubes with 17 microchannels, with internal dimensions of 0.60 x 0.43 mm<sup>2</sup>. In the first pass the refrigerant enters through the left side in the upper region and is distributed through 44 tubes that cross the heat exchanger. After the first pass, the refrigerant flows through a filter drier, which removes any impurities or moisture from the system, and continues to the second pass. This second pass has eight tubes through which the refrigerant flows towards the heat exchanger outlet, located on the lower left side. The condenser model is also divided into three regions: cooling ( $r_1$ ), condensation ( $r_2$ ) and subcooling ( $r_3$ ). In the first region ( $r_1$ ), the superheated refrigerant fluid that leaves the compressor is cooled until it reaches the saturated vapor state. In the second region ( $r_2$ ), identified as the condensation region, the fluid continues the heat rejection process until it reaches the saturated liquid state. Finally, in the third region ( $r_3$ ), the fluid is cooled below the saturation temperature, at which point it reaches the subcooled liquid state. The position of the two boundaries that separate these three regions is part of the solution to the mathematical model. The condenser submodel was solved iteratively based on the effectiveness-NTU method (Çengel and Ghajar, 2020).

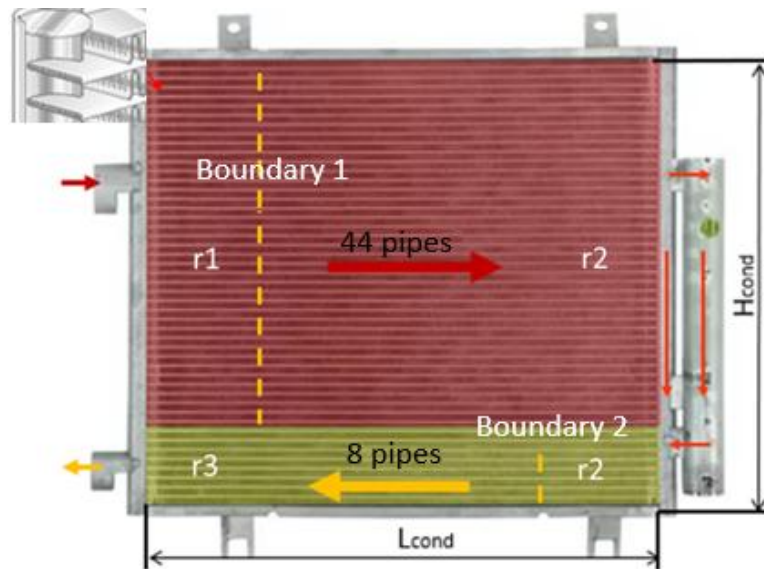


Figure 3. Microchannel type condenser and detail of flat tubes.

The number of transfer units ( $NTU$ ) is calculated as the ratio between the overall coefficient of the heat exchanger and the minimum heat capacity between the two flows, which is described by:

$$NTU = \frac{UA}{\dot{C}_{min}}, \quad (7)$$

where the overall heat transfer coefficient, consider the air side, refrigerant side and wall side thermal resistances, being evaluated as

$$\frac{1}{UA} = \frac{1}{\eta_{air} h_{air} A_{air}} + \frac{\delta_w}{\kappa_w A_w} + \frac{1}{h_{ref} A_{ref}}. \quad (8)$$

### 3.2.1 AIR SIDE

Wang *et al.* (1999) correlation is used to calculate the Colburn factor ( $j$ ) on the air side, expressed by

$$j = 0.324 Re_{Dc}^{j_1} \left(\frac{F_p}{P_t}\right)^{j_2} (\tan\theta)^{j_3} \left(\frac{P_l}{P_t}\right)^{j_4} NF^{0.428}, \quad (9)$$

allowing the evaluation of the convective heat transfer coefficient of the airflow.

The fin efficiency ( $\eta_{fin}$ ) was also considered to calculate the overall effectiveness of the finned surface, expressed by

$$\eta_{air} = 1 - \frac{A_{fin}}{A_{ext}} (1 - \eta_{fin}). \quad (10)$$

### 3.2.2 REFRIGERANT SIDE

The internal convective heat transfer coefficient of the refrigerant in the cooling region ( $r_1$ ) and subcooling region ( $r_3$ ) were evaluated with the Gnielinski's correlation (Çengel and Ghajar, 2020), expressed by

$$Nu_{r1,r3} = \frac{(f/8)(Re_{r1} - 1000) Pr_{r1}}{1 + 12.7(f/8)^{1/2} (Pr_{r1}^{2/3} - 1)}. \quad (11)$$

In turn, in the condensation region, where the phase change occurs, the internal convective heat transfer coefficient was evaluated by Klimenko (1988) correlation

$$Nu_{r2} = 0.05 Re_{r2}^{0.5} Pr_{r2}^{0.33}. \quad (12)$$

### 3.2.2 CONDENSER HEAT TRANSFER

After the heat transfer coefficients of each region have been determined, Eq. (8) is solved and the effectiveness-NTU method is used to determine the region of the condenser occupied by each of the three regions. It results in an iterative procedure that allows the quantification of the total heat transfer rate of the condenser, expressed by

$$\dot{Q}_{cond} = \dot{Q}_{r1} + \dot{Q}_{r2} + \dot{Q}_{r3}. \quad (13)$$

### 3.3 EVAPORATOR

The mathematical solution of the evaporator is performed in the last part of the calculation procedure to define the evaporator's cooling capacity, and is presented as

$$\dot{Q}_{evap} = \dot{m}_r (i_{evap,out} - i_{evap,in}), \quad (14)$$

where the refrigerant mass flow rate was calculated by the compressor submodel (Eq. 3), the enthalpy at the evaporator inlet is obtained by the enthalpy at the condenser outlet assuming an isenthalpic process and the enthalpy at the evaporator outlet is experimentally obtained or considered an input.

### 3.4 SOLUTION PROCEDURE

The flowchart for solving the computational model of the AC system is shown in Fig. 4. The model's input parameters are initially considered, namely air temperature and relative humidity, vehicle speed, subcooling and superheating temperature, suction pressure, compressor rotation, and evaporator air flow. Next, an estimate for the refrigerant pressure in the condenser is also provided to the model. Then, the calculation procedure moves on to the compressor model to obtain the refrigerant mass flow rate, power consumption, and discharge temperature.

In the condenser, the mathematical model calculates the positions of the interfaces among different regions of the condenser, refrigerant temperature at its outlet and the rejection heat rate. Additionally, the Newton-Raphson computational method is used to determine the air mass flow rate in the three regions of the condenser (Vargas and Araki, 2016).

After the condenser pressure is determined, the calculation procedure moves on to the evaporator to determine the system's refrigeration capacity, which, when combined with the compressor's power consumption, allows the calculation of the system's coefficient of performance. This procedure was implemented on Engineering Equation Solver software and is repeated until the energy conservation principle of the entire system has been achieved.

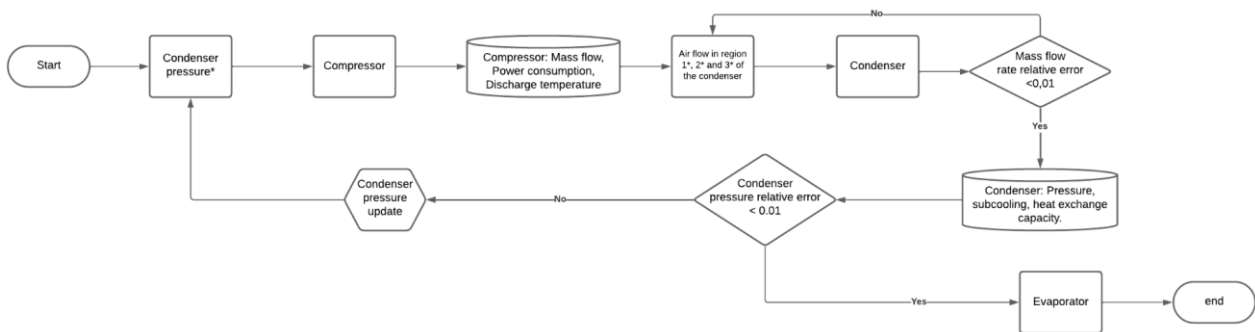


Figure 4. Flowchart of the computational model.

## 4. RESULTS

This section presents the results of the validation exercises for the compressor and AC system model, compares the AC system performance using refrigerants R-134a and R-1234yf, and provides a comparative analysis of different condenser fin densities.

### 4.1 COMPUTATIONAL MODEL VALIDATION

Using the dataset collected according to the experimental plan outlined in Table 1, the coefficients in Eq.2 and Eq. 6, used to model compressor performance, were regressed. Figure 5a compares the compressor isentropic efficiency obtained experimentally and predicted by the compressor submodel. As can be seen, all predictions presented errors of less than 10.0% in relation to the experimental data. For isentropic efficiencies values below 65.0%, the model showed a slight tendency to overestimate the results with a margin of less than 10.0%. Moreover, Figure 5b shows a comparison between the compressor volumetric efficiency, where can be seen that the simulated results showed values very close to the experimental results with errors of less than 5.0%. Thus, the compressor submodel demonstrated good accuracy in predicting the volumetric and isentropic efficiencies under the various experimental conditions evaluated.

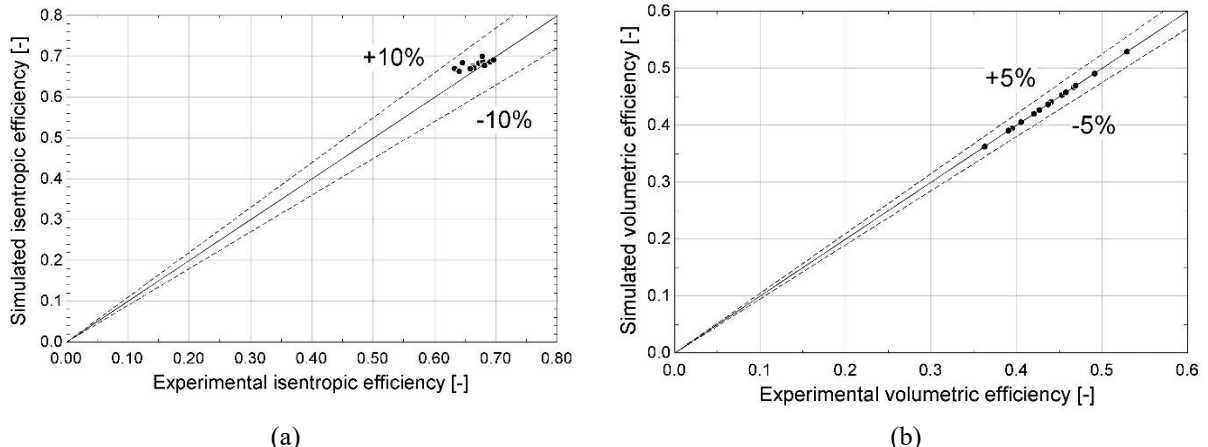


Figure 5. Compressor experimental and simulated isentropic efficiency (a) and volumetric efficiency (b).

After the compressor submodel has been validated, the complete AC system model was assessed by comparing the predictions of the discharge pressure and the evaporator cooling capacity with the experimental database. Figure 6a demonstrates the high accuracy of the model in predicting the compressor discharge pressure, equivalent to the condenser inlet pressure, with all but one experimental point falling within the  $\pm 5.0\%$  error band. Furthermore, Figure 6b shows that the model was able to predict the cooling capacity with differences smaller than  $\pm 10.0\%$  for most of the experimental conditions. Only two points, with cooling capacity under 2500 watts, presented values with errors above  $\pm 10.0\%$  and smaller than  $\pm 20.0\%$ . These larger errors are mainly justified by the lack of experimental compressor performance points for low-capacity conditions.

Figure 7 shows experimental and computational results related to compressor power consumption. Within the range of values analyzed, it is observed that the results of the model expressed values very close to the center line, causing errors lower than  $\pm 10.0\%$  in relation to the experimental database. Thus, the validation exercise demonstrated that the good accuracy of the complete AC system model to predict the main performance indicators of an automotive air-conditioning system, such as discharge pressure, cooling capacity and compressor power consumption.

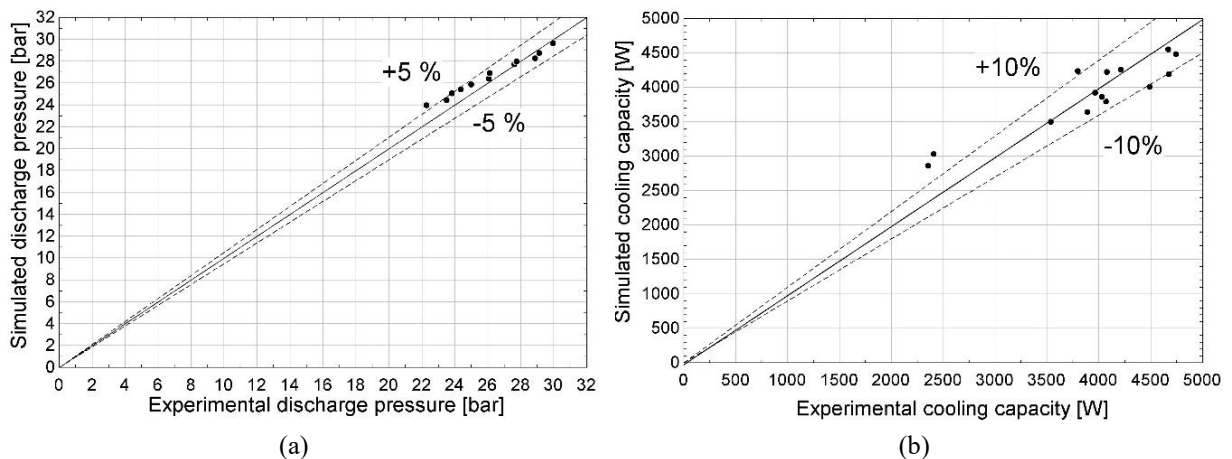


Figure 6. Comparison of experimental and simulated discharge pressure (a) and cooling capacity (b).

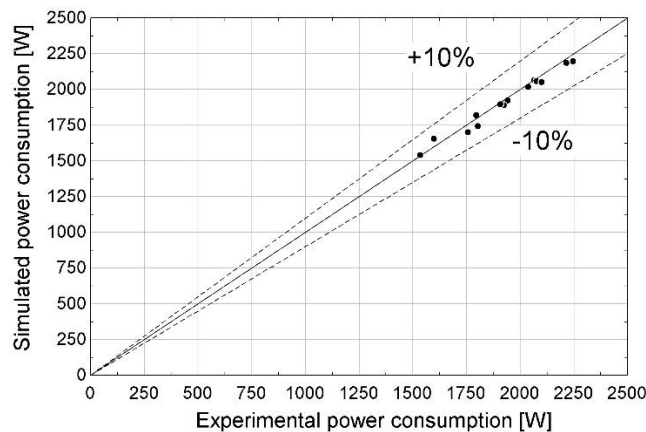


Figure 7. Experimental and simulated compressor power consumption.

#### 4.2 COMPARISON OF R-134a AND R-1234yf

After the validation exercise, the model was used to evaluate the performance of the AC system using refrigerant R-1234yf. Simulations were carried out using evaporating temperature, subcooling degree and supercooling degree of 2.5 °C, 15.0 °C and 10.0 °C, respectively. These values were defined based on the experimental activity of this work and are representative for automotive AC applications (SAE, 2017). Figure 8a provides a comparison between thermodynamic properties of refrigerants R-134a and R-1234yf. It is observed in Fig. 8a that the two refrigerants have analogous saturation pressures, with differences lower than 0.5 bar. This similarity between the thermodynamic properties of these two refrigerants is one of the aspects that favors R-1234yf as a potential low GWP option to replace R-134a. On the other hand, Fig. 8b shows that R-1234yf exhibits a latent heat of vaporization ( $i_{vap}-i_{liq}$ ) approximately 20% lower than that of R-134a.

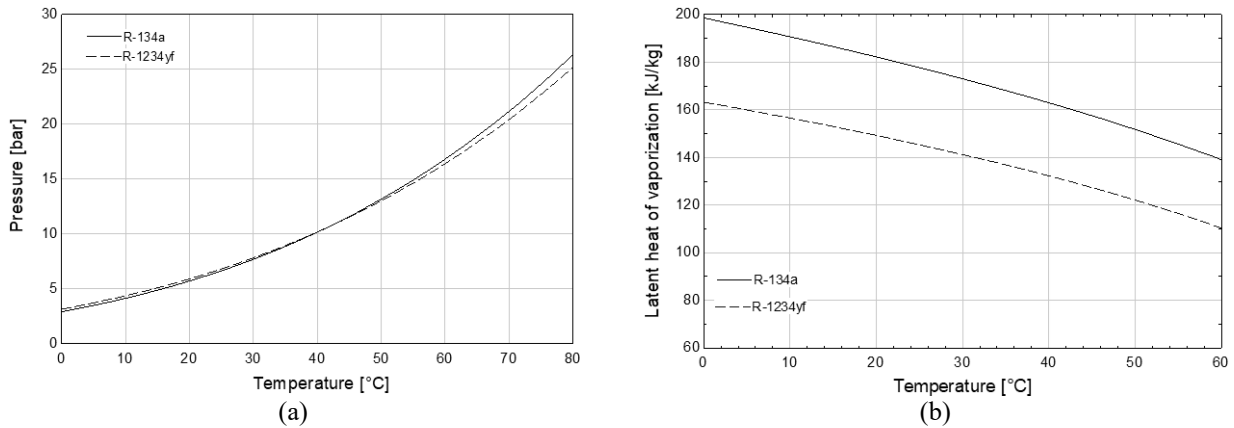


Figure 8. Saturation pressure (a) and latent heat of vaporization (b) as a function of temperature.

Figure 9a shows a comparison between the simulated cooling capacities of R-134a and R-1234yf, as a function of the ambient temperature. The observed reduction in the cooling capacity for both refrigerants, as the ambient temperature increases, is mainly justified by a reduction in the compressor mass flow rate, which in turn reduces the cooling capacity. When comparing the refrigeration capacity of the two refrigerants, it is observed that the R-1234yf showed a 5.8% average reduction. This drop in the refrigeration capacity of R-1234yf in relation to R-134a is mainly due to the lower latent heat of vaporization of R-1234yf. Figure 9b shows the COP as a function of ambient temperature. It is observed that the COP of the refrigerant R-1234yf showed an average drop of 2.6% compared to the fluid R-134a, mainly justified by the reduction in cooling capacity.

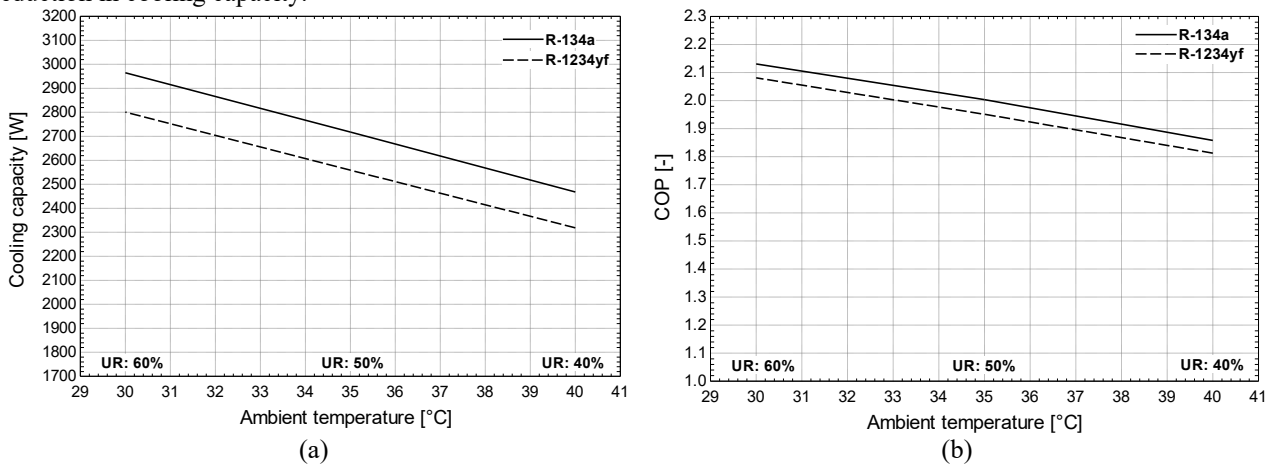


Figure 9. Cooling capacity (a) and COP (b) as a function of ambient temperature.

Figure 10 shows a comparison between R-134a and R-1234yf, regarding the cooling capacity and the compressor power consumption for different compressor speeds. Considering the compressor speed to 2000 rpm, it is calculated a reduction in the refrigeration capacity of R-1234yf of 6.0% compared to R-134a. For the same speed, the compressor power consumption showed a drop of 3.7% for the refrigerant R-1234yf compared to R134a. Although the use of R-1234yf led to a reduction in compressor power consumption, it was insufficient to offset the decline in cooling capacity, resulting in a 2.5% decrease in the COP of the system operating with R-1234yf.

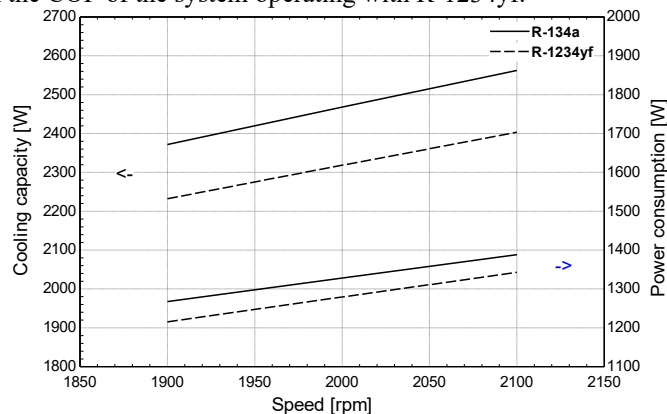


Figure 10. Cooling capacity and compressor power consumption as a function of compressor speed.

The computational model was subsequently used to investigate a strategy for mitigating the COP reduction resulting from replacing R-134a with R-1234yf. Specifically, simulations were conducted with varying fin density to increase the condenser's heat exchanger area without altering its external dimensions, which is a frequent restriction in automotive AC design. As shown in Figure 11a, increasing the fin density led to a consistent reduction in compressor discharge pressure across the entire velocity range analyzed. This effect is attributed to the larger surface area, which allows the condenser to reject an equivalent amount of heat at a lower temperature, thereby reducing system operating pressure. Figure 11b illustrates the corresponding improvement in system performance, showing a COP increase of approximately 1% when fin density is raised from 1000 to 1200 fins/m. These findings emphasize the value of the computational model for evaluating different refrigerants or modifications on components of the AC system.

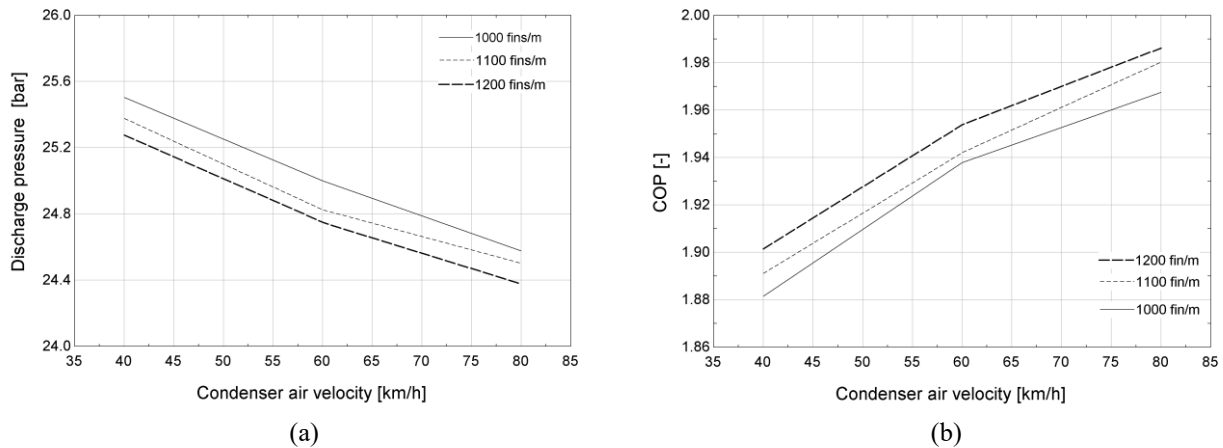


Figure 11. Discharge pressure (a) and COP (b) as a function of condenser air velocity.

## 5. CONCLUSIONS

This work presented an experimental and computational analysis of the thermal performance of an automotive air-conditioning system. Based on the study, the following conclusions can be drawn:

- Validated computational models, when supported by reliable and representative experimental data, are essential tools for the development of automotive AC systems.
- Such models can effectively be adapted to assess the performance of alternative refrigerants and system parameters, reducing the reliance on extensive experimental testing.
- Although R-134a and R-1234yf presented the same trends in relation to the model input variables, the results for the R-1234yf fluid showed a reduction in the refrigeration capacity in the range of 6% and a reduction in the COP of 2.5%.
- The proposed model showed the ability to assess new design geometries that could help offset part of the COP reduction observed in R-1234yf, such as using a condenser with a larger heat transfer surface.

## 6. REFERENCES

- Cordova, G.M., 2024. "Experimental and computational evaluation of automotive air-conditioning systems operating with R-134a and R-1234yf (in Portuguese)". Master's thesis, Federal University of Santa Catarina, Joinville, Brasil.
- Çengel, Y.A., Ghajar, A.J., 2020. "Heat and Mass Transfer - Fundamentals and Applications". 6<sup>th</sup> Edition, McGraw-Hill Education, New York, NY.
- Da Silva, D.L., De Oliveira, I.S., Juliani, A.D.P., Cordova, G.M., 2024. "Automotive air-conditioning system thermal performance assessment: an experimental approach combining first and second laws of thermodynamics". *Journal of the Brazilian Society of Mechanical Sciences*, v. 46, p. 703 (<https://doi.org/10.1007/s40430-024-05283-1>).
- Da Silva, D.L., Melo, C., 2016, "A Perspective on R&D&I Activities in the Brazilian Mobile Air Conditioning Market", *In Proceedings of the 16th Brazilian Congress of Thermal Sciences and Engineering, ENCIT 2016*, Vitoria-ES (10.26678/ABCM.ENCIT2016.CIT2016-0650).
- Da Silva, D.L., Cordova, G.M., 2017, "Mathematical Model of an Automotive Air-Conditioning System under Steady-State Conditions". *In Proceedings of the 24<sup>th</sup> ABCM International Congress of Mechanical Engineering* (10.26678/ABCM.COBEM2017.COB17-0367).
- Hermes, C.J.L., Silva Jr., W.L., Castro, F.A.G., 2012, "Thermal-hydraulic design of fan-supplied tube-fin condensers for refrigeration cassettes aimed at minimum entropy generation". *Applied Thermal Engineering*, v. 36 (2012) 307e313.
- Kigali, 2024, *Kigali Amendment*, 2024. [https://treaties.un.org/Pages/ViewDetails.aspx?src=IND&mtdsg\\_no=XXVII-2-f&chapter=27&clang=\\_en](https://treaties.un.org/Pages/ViewDetails.aspx?src=IND&mtdsg_no=XXVII-2-f&chapter=27&clang=_en), Accessed 31 May 2024.

- Klimenko, V.V., 1988, “A generalized correlation for two-phases forced flow heat transfer: second assessment”. *International Journal of heat and mass transfer*, v. 31, p. 541–552.
- Lahimer, A.A., Razak, A.A., Sharol, A.F., Sopian, K., 2023. “Automotive cabin soak temperature control strategies for improved safety, comfort and fuel efficiency: A review”. *Solar Energy*, 259 (2023) 416–436.
- Li, W., 2013. “Simplified steady-state modeling for variable speed compressor”. *Applied Thermal Engineering*, v. 50. 318-326.
- Liu, H., Wang, S., Su, Q., 2025. “Characteristics optimization of automotive air conditioning based on dynamic thermal comfort in complex thermal environment”. *Thermal Science and Engineering Progress*, v. 60 (2025) 103430.
- Mendes, R.P., Pábon, J.J.G., Pottie, D.L.F., Machado, L., 2024 “Artificial intelligence strategies applied in general and automotive air conditioning control. A review of the last 20 years”, *Int. Journal of Refrigeration*, v. 164, 180-198.
- SAE (2017) J2765 - Procedure for measuring system COP [Coefficient of Performance] of a Mobile Air-Conditioning System on a Test Bench, *SAE International*.
- Vargas, J.V.C, Araki, L.K., 2016. “*Cálculo numérico aplicado*” 1<sup>a</sup>. ed, Editora Manole.
- Vashisht, S.; Rakshit, D. 2021. “Recent advances and sustainable solutions in automobile air conditioning systems”. *Journal of Cleaner Production*, v. 329.
- Zhan, C., & Yu, J., 2022. “Integrated simulation of refrigerant flow and thermal comfort in automotive climate control systems”. *SAE Technical Paper*, 2022-01-0356.
- Zhang, Z.; Wang, J.; Feng, X.; Chang, L.; Chen, Y.; Wang, W., 2018. “The solutions to electric vehicle air conditioning systems: a review”. *Renewable and Sustainable Energy Reviews*, v. 91, p. 443–463.
- Wang, H., Wang, Y., & Wang, X., 2019. “Numerical simulation and experimental validation of automotive air conditioning system performance”. *Applied Thermal Engineering*, 147, 547-557.
- Wang, C.C., Jang, J.Y., Chiou, N.F., 1999, “A heat transfer and friction correlation for wavy fin-and-tube heat exchangers”. *Int. J. Heat Mass Transf.*, v. 42, p. 1919–1924.

## 7. RESPONSIBILITY NOTICE

The authors are the only responsible for the printed material included in this paper.